An Investigation on 3d Printing Board Lattice Structure Material

Abstract

Structural lightweight design is the process of reducing the amount of material in a component to reduce its overall weight without sacrificing reliability or function. It is the most common application in aerospace, automotive manufacturing and Marine ships, and has received extensive attention from the industry and academia. TPMS combined with 3D printing technology can realize the integrated production of porous structures, solve the problem of processing micro-size material components, and is an important technical support in the process of structural lightweight. In this paper, by designing different TPMS porous structures and optimizing the 3D printing parameters process, polylactic acid (PLA) was successfully printed by material fusion deposition molding (FDM) method, and the tensile and compression characteristics of different structures were analyzed through mechanical properties testing.The experimental results show：

(1) The print specimen is divided into three stages in the whole tensile process, which are elastic stage, yield stage and fracture stage, and the failure form is brittle failure. Among them, the tensile properties of D structure are the best, while the tensile properties of F-RD structure and N structure are relatively poor.

(2) The printed specimen has two forms in the whole compression stage process, FRD structure and D structure have three stages, that is, the rising stage, the gentle stage, the second rising stage, and the N structure has only two stages, that is, the rising stage and the second rising stage. Among them, F-RD structure and D structure have relatively good compression performance,The shape variables are all about 55% under 13MPa,while N structure has poor compression performance,At 13MPa, the shape variable is only 15%.

(3)The type D sample has horizontal pore type, the more uniform the stress is, and the lower the number of stress concentration sites in the same position interface, the better tensile and compressive properties. FRD sample has large pores, but the number is small, the force is more uniform, and the overall tensile and compressive properties are slightly lower than D sample. N-type samples have the largest number of pores, small pores and large distribution area. In the same section, there are many stress concentration locations, which seriously affect the tensile and compressive properties, so the N-type tensile and compressive properties are the worst.

Keywords: 3D printing , Aerospace, Automotive Manufacturing, Fusion Deposition Molding (FDM), Mechanical property, Marine Ships, TPMS model

1Introduction

"3D printing", known academically as "rapid prototyping" or "additive manufacturing", is a high-tech manufacturing technology that emerged in the late 1980s and early 1990s. It is a process of building components layer by layer using 3D design data. Unlike traditional manufacturing techniques,3D printing is a bottom-up

process that offers more design freedom and the ability to create complex tissues without the need for molds and tools. As a result, 3D printing has been recognized as an efficient and fast manufacturing technique for realizing digitally modeled geometric objects in a variety of industries, including chemical, mechanical, automotive, aerospace, electrochemistry, electronics, and biomedical engineering. The 3D printing market has grown significantly over the past 10 years at an average rate of about 26% per year[1].

The development of 3D printing technology benefits from the integration of modern CAD/CAM technology, mechanical engineering, layered manufacturing technology, laser technology, computer numerical control technology, precision servo drive technology and new material technology[2]. Its basic principle is to use layered manufacturing and layer-by-layer superposition to achieve the production of objects, which is similar to the integration process in mathematics. In the process of 3D printing, the printer is connected to the computer, the printing method and parameters are set through the computer software[3], the cross-section shape of the workpiece is formed by scanning in the XY plane, and then the printing materials are gradually stacked layer upon layer according to the Z coordinate interval to realize the transformation of the design drawings on the computer into solid objects. Because the final product is obtained by gradually adding materials and stacking them layer by layer, 3D printing technology is also often referred to as additive manufacturing technology.

Fused deposition molding (FDM) : Fused deposition molding is a 3D printing technology widely used in rapid prototyping and custom production[4] .Thermoplastic filament is used as the starting material and fused and extruded for layer upon layer bonding to create 3D objects. In the FDM process, computer aided design software first cuts the 3D model into thin layers and generates path data for each layer. The printer then heats the thermoplastic material (such as PLA, etc.) from the nozzle to the melting temperature, and piles it up layer by layer on the printing platform in a predetermined path by moving the nozzle, while cooling and curing between each layer. Hot melt extrusion technology is often used in combination with FDM technology to melt and mix drugs and excipients together in the extruder to produce high-quality intermediate filaments for subsequent preparation. Some polymers commonly used in filaments preparation include polyethylpyrrolidone (PVP) and polylactic acid (PLA)[5]. As a mature 3D printing technology, melt deposition molding has a wide range of application prospects in industrial manufacturing, education and individual makers. The FDM printing principle is shown in Figure 1.

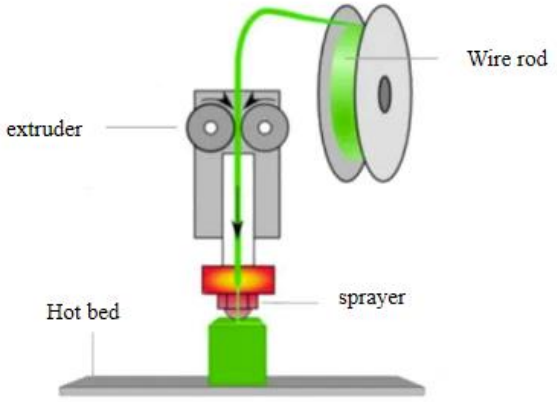

Figure 1 FDM printer principle

Porous structure is a bionic structure with natural advantages, including a large number of pore structures, with low relative density, high specific surface area, good permeability[6], lightweight and other advantages, widely used in aerospace, automotive manufacturing, material chemistry, medical and other engineering fields. Among them, the open pore structure has connected channels, so it has a wider applicability in various applications. Common porous structures include lattice structures, honeycomb structures and three-period minimal surfaces. In recent years, three-period minimal surface structures (TPMS) have attracted more and more attention because of their unique characteristics. The three-period minimal surface has the advantages of diverse geometric shapes, high specific surface area, fully connected pores, controllable parameters and quasi-self-supporting, so it is widely used in energy-absorbing structure and bone scaffold modeling. There are many types of porous models, which can be formed by randomly distributing voids in space or according to specific laws, or by methods such as function surfaces. In this paper, we choose the thicker triply periodic minimal surface TPMS as the basis of the porous model[7].

Minimal surface is a geometric structure whose mean curvature is zero, which makes it have excellent mechanical and structural properties. Rashid K et al.[8] used selective laser sintering (SLM) technology to prepare super-strong steel (i.e. maraging steel) and successfully created micro-scale curved structures. Maskery[9] et al. designed the volume fraction of lattice structures by using the surface equation of structures, and established the relationship between the volume fraction of materials and the elastic modulus of lattice structures, which provided a method for designing lattice structures with specific stiffness. Over the past three centuries, this structure has been extensively studied, especially in the fields of mathematics and computer graphics. This geometry can be defined mathematically and porous structures with three-dimensional continuous full connections can be designed. In addition, due to its exquisite design and smooth curve characteristics, minimal curved surface has been widely concerned in the field of architectural design, and has been widely recognized in practical applications. As shown in Figure 2, the Astana Expo, located in Kazakhstan, is a design application of minimal curved surfaces [10].

Figure 2. Minimal curved architecture

Up to now, many people have studied the mechanical properties of PLA.In order to improve the inherent brittle-ability of PLA and expand its application range, a new biobiofuran diformate (DAF) plasticizer with novel structure was designed and synthesized by esterification of 2, 5-furan diformate and natural fatty alcohols. The plasticizing behavior and mechanism of DAF on PLA were studied by means of tensile properties test, melt crystallization behavior analysis, thermogravimetric behavior analysis, dynamic mechanical properties analysis and microscopic morphology analysis. It was found that DAF showed a good substitution effect for DOTP in plasticized PLA[11].Orisekeh[12] et al. studied egg shell particles (ESP) as inorganic calcium carbonate fillers to enhance the mechanical properties of PLA. Eggshell powder enhanced the dynamic mechanical properties of PLA, where 3 wt% concentration had the highest energy storage modulus at room temperature, and the energy storage modulus of filament and 3D printed sample was increased by 5.2 % and 3.6 %, respectively. Finally, eggshell particles had little effect on the tensile and bending strength of the composite, but increased the compressive strength of PLA. The average strength and modulus of the 5 wt% sample were 66.50 MPa and 2.27 GPa, respectively.Li[13] et al. used polylactic acid (PLA) as a 3D printing melt deposition forming (FDM) material, took tensile strength as an optimization index, and systematically studied the influence of four process parameters, namely printing layer thickness, printing Angle, filling density and printing temperature, on the tensile strength of PLA parts through single factor test and response surface method. With the help of Design-Expert software, variance analysis and parameter optimization were carried out to obtain the optimal combination of molding process parameters and verify the correctness of the test results. The results show that when the thickness of the printing layer is 0.2mm, the printing Angle is 70°, the filling density is 70%, and the printing temperature is 200℃, the mechanical properties of the specimen are the best.Li[14] et al. addressed this gap by using computational fluid dynamics (CFD) to investigate the effect of isosurface migration on the mass transfer performance of the three TPMS stents (Fisher-Koch S, Gyroid, and Split-P).The above are traditional mechanical analysis of fixed models alone, without taking into account factors such as holes. This experiment will focus on exploring the influence of hole characteristics on mechanical properties.

The holes of N-type porous surface are larger square, and the connectivity is poor[15].Most of the holes in the D-type surface model have good horizontal

connectivity[16].The holes of the FRD surface are all round, which is conducive to heat conduction[17].In this paper,in order to better analyze the mechanical properties of the tmps structural model, we choose three representative tmps functions,FRD-type, D-type and N-type porous surfaces in TMPS are selected as research objects, and the models are printed by FDM3D printing technology, and their mechanical properties are analyzed.The holes of these three models are unique, which is helpful to analyze the influence of the hole linkage characteristics on the mechanical properties, and further help us to analyze and understand the tmps model.

2 Methodology:

2.1 3D printing materials

Polylactic acid (PLA) is a popular 3D printing material that is favored for its unique properties[18]. First, it has excellent stiffness and strength, making the printed parts strong and durable. Secondly, PLA is easy to process and can be made into a variety of shapes, from simple components to complex structures[19]. PLA is also a biodegradable material, which means that under certain environmental conditions, it can be broken down naturally, reducing the negative impact on the environment. Because PLA generally does not contain toxic substances, it is also more common in fields such as food packaging and medical devices. Although it softens at high temperatures, PLA still has certain thermal stability, making it more widely used in low temperature environments. Overall, PLA has shown broad application potential in many industries due to its excellent mechanical properties, processing convenience, biodegradability and high safety. The material used for 3D printing in the experiment is PLA filament. Table 1 lists the specific material parameters.

Table 1 Material properties of PLA

Materials	Density /g*cm-3	Poisson's ratio	Young'smodulus /GPa	Yieldstrength /MPa
PLA	1.24	0.38	3.5	60

2.2Build a model

In this paper, three-period minimal surface is used as the sample model. Since three-period minimal surface is usually modeled by implicit function, and common computer-aided design software (CAD) has difficulties in the accuracy of establishing three-period minimal surface model, therefore, In this paper, Blender software with the function of accurately designing three-period minimal surface was selected to build the model. Blender software shows remarkable efficiency in building three-period minimal surfaces (a complex surface with specific mathematical properties). It provides advanced modeling techniques and toolsets that enable engineers and designers to create these types of surface models quickly and accurately. As a software designed specifically for 3D modeling, Blender is not only good at handling complex geometric forms, but also ensuring that these forms are translated into designs with actual manufacturing value. Compared to other modeling software,

Blender has a significant advantage when it comes to building three-period minimal surfaces. Its flexible adjustment function allows users to precisely control the curvature and shape of the surface to meet specific design needs, while maintaining the detail richness and smoothness of the surface. This makes Blender ideal for dealing with this type of complex surface design. Through Blender modeling software, import the corresponding TMPS type function, you can build the model.The TPMS model function used in this paper is shown in Table 2 below, and the model built by Blender is shown in Figure 3.

Table 2 Mathematical functions of FRD, N and D surfaces[20]

TMPS	Mathematical function
FRD	$f(x,y,z)=\cos(\omega_x x)\cos(\omega_y y)\cos(\omega_z z)+\cos(2\omega_x x)\cos(2\omega_y y)\cos(2\omega_z z)-\cos(2\omega_x x)\cos(2\omega_y y)-\cos(2\omega_x x)\cos(2\omega_y y)-\cos(2\omega_x x)\cos(2\omega_z z)=C$
D	$f(x,y,z)=\cos(\omega_x x)\cos(\omega_y y)\cos(\omega_z z)-\sin(\omega_x x)\sin(\omega_y y)\sin(\omega_z z)=C$
N	$f(x,y,z)=3\{\cos(\omega_x x)+\cos(\omega_y y)+\cos(\omega_z z)\}+4\cos(\omega_x x)\cos(\omega_y y)\cos(\omega_z z)=C$

Let ω = 1.0. The key parameters of each TPMS structure, including specific surface area and porosity, are independent of the ω value and instead depend on the corresponding C value. The values of the various design parameter C used in this study, along with the associated main structural parameters, are presented in Table 3.

Table 3 Multi-surface model parameters

TPMS	Paramter C	Dimension (cm)	Surface Area(cm^2)	Volume (cm^3)	Porosity (%)	Specific surface area(cm^2/cm^3)
FRD	0.5	4×4×4	252.8271	20.2806	68.31	12.466
N	0.25	4×4×4	290.3272	31.4629	50.84	9.2276
D	0	4×4×4	244.7745	31.7569	50.38	7.707

It can be seen from the table that the hole rate of the N-type model is similar to that of the D-type model, but the specific surface area of the N-type model is larger. The surface area of the N-type is the largest, indicating that the number of internal holes is relatively large. The surface area of FRD type is similar to that of D type, but the FRD porosity is relatively large, indicating that FRD type porosity is large, but the number is small.

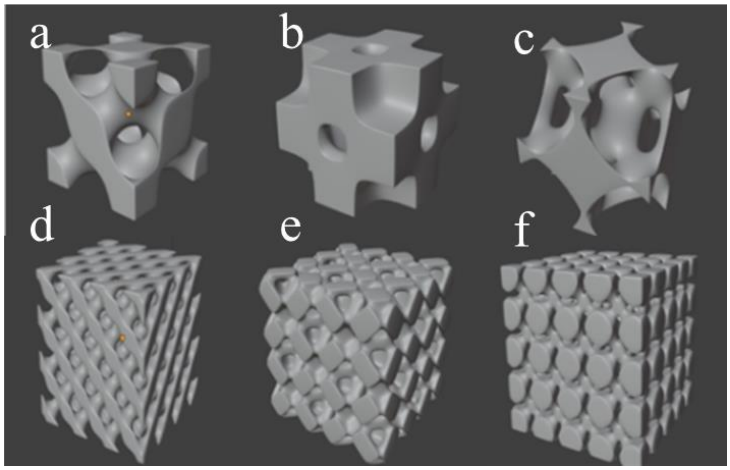

Figure.3. (a-c) D, FRD, N single cell model; (d-f) D, FRD, N model diagram

2.3 Setting of slicing and printing parameters

Based on the experience analysis of unsuccessful printing before, we finally determined the best printing parameters in this experiment, as shown in Table 4. This paper mainly discusses how to use this optimum printing parameter to improve the surface quality and adhesion of the metal sheet on the hot melt layer. First, in order to make the specimen adhere more efficiently to the hot bed surface, we initially decided on a slower printing speed, which reached 30mm/s. The height of each layer was also set to 1mm, and in addition, we utilized Raft as an attachment platform. At other levels, the printing rate is 40mm/s, but the vertical height of this layer remains constant. This approach not only enhances the stability of the first layer, but also guarantees the overall efficiency of the printing process. The platform temperature is 60℃ and the filling rate is 100%.

Table 4 Print parameter Settings

Print speed （mm/s）	Initial print spee （mm/s）	Attachment platform type	Layer thickness （mm）	Packing density （%）	Print temperature /（℃）	Platform temperature/ （℃）
50	30	Raft	1	100	210	60

2.4 The adhesion surface of the sample was improved

In the process of printing, it is easy to appear the adhesion surface is not firmly attached, resulting in the sample printing failure, which is due to the hot bed temperature is too high, and the printing model is too stressed, resulting in the model adhesion loose. This condition will result in incorrect specimen printing position. Problems shown in Figure 4. In order to avoid this problem, the temperature of the hot bed can be reduced, and the solid glue can be applied evenly on the hot bed before printing, so that the printed sample is firmly bonded to the hot bed.

In addition, when printing, FDM printing wire is very smooth, no other problems. The printing process nozzle is carried out in strict accordance with the model slicing programming code. (The slicing software used is UltimakerCura)

Figure 4 Adhesion loosening of the sample

1、Mechanical property test and result analysis

3.1 Material properties test method

In order to explore the mechanical properties of the material, in this test, according to the national standard GJB770B – 2005[20], an electronic universal testing machine is used to carry out a uniaxial tensile test on the specimen, and the mechanical properties of the material are evaluated by observing the P-Δl curve and fracture appearance, combined with the performance index. We have carried out tensile and compression experiments on the lattice structure, from which the relationship between load and displacement and deformation image data are obtained, aiming to explore the deformation mode and energy absorption characteristics of the lattice model under the environment of tensile and compression. Tensile and compression experiments were carried out on the TMPS structure samples, and the test was carried out by displacement controlled loading method, and it was ensured that one test was carried out in each model experiment to ensure the accuracy of the data. The force sensor on the test machine captures the loading force of the specimen during the stretching and compression process.

3.2 Experimental equipment and operation process

In this experiment, we used the WDW microcomputer controlled electronic universal testing machine, which is a test equipment specially used to evaluate the mechanical properties of metal and non-metal raw materials and finished semi-finished products in tensile, compression, bending and shear. It can simultaneously measure the mechanical properties of many materials. This technology is mainly used in a number of mechanical testing centers, such as in the iron and steel metallurgy industry, where it is often used to test the physical properties of thin sheets and small and medium diameter metal materials. The test system is composed of three parts: data acquisition system, control system and display system. The device uses a four-column frame design, combined with a high-precision ball screw drive and load sensor, to enable precise loading of samples. At the same time, the system is driven by stepping motor, and the step Angle is changed by software programming, so as to achieve the required load value. The transmission system uses the servo drive and servo motor of Panasonic Japan, as well as the imported reducer and synchronous

gear belt to achieve the loading operation. At the same time, the equipment has high reliability and good maintainability, and can meet the requirements of different specifications of samples. In addition, this equipment is also equipped with a microcomputer control system, so as to achieve the entire test process of automatic management, the testing machine can be remotely controlled and data transmission through the upper computer.

Figure.5.WDW microcomputer control electronic universal testing machine

Experimental steps:

Boot the operating system and generate a new compressed file. Through the measured data, the load and strain values required to be applied to the die after the specimen deformation are determined. The properties of the material are added to the model and the area of the force on the model is estimated. Start the computer loading program, apply different pressures to test the specimen, and record the data at each time point. Then, put the specimen into the test machine and make sure that there is a slight contact between the model and the load sensor on the test machine. After setting up, start the loader to perform the experiment. Next, we set the experimental conditions in the software: the pressure is set to 2000N, the compression rate is 2.4mm/s, and the displacement control strategy is selected. When the sample is completely pressed in, close the valve and stop loading. Click the Start experiment button on the software interface to start the compression process of the model, and make its deformation amplitude reach 65% until the compression task is complete. Finally, the experimental data will be saved. The same is true for the tensile experiment. The material properties are introduced, the sample is clampped with a fixture, and the experimental parameters are set in the software: the tensile force is set to 2000N, the tensile speed is 1mm/s, and the displacement control mode is selected. Click Start experiment on the software, start stretching the model, make it break, complete the stretching experiment, and finally save the experimental data.

3.3 Result and Discussion:

3.3.1 Tensile test results

Table 5 is the main parameters of the tensile sample, and Figure 6 is the legend of the tensile sample, which can be seen in strict accordance with GJB770B-2020.

Table 5 Model parameters of tensile specimen

TMPS MODEL	SINGLE CELL SIZE /MM	POPULATION SIZE /MM	BULK VOLUME /MM3
D	2×2×2	115×25×2	3603
N	2×2×2	115×25×2	3603
F-RD	2×2×2	115×25×2	3603

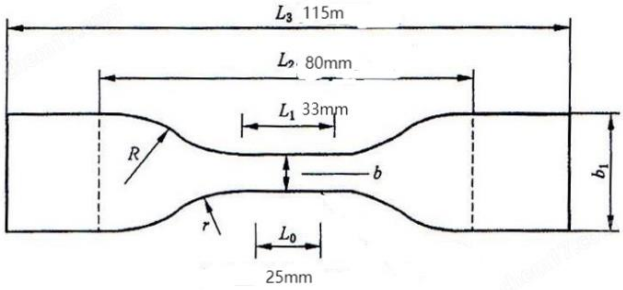

Figure.6. Tensile specimen

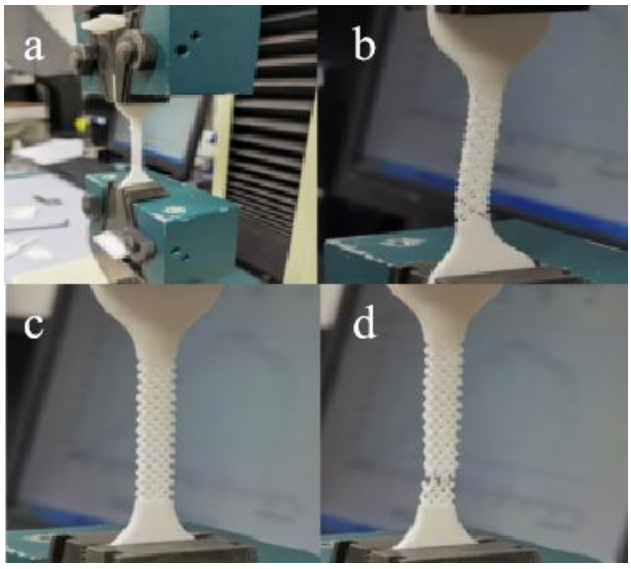

Figure.7.(a)Before the D-stretch;(b)After the D-stretch;(c)Before the N-stretch;(d)After the N-stretch

Table 6 tensile sample data table

TMPS Model	Elastic phase maximum displacement（mm）	Maximum load in elastic phase （N）	Fracture displacement （mm）	Breaking load （N）
FRD	2.4	25	3.9	24
N	1.6	11	3.0	10
D	1.6	82	5.7	75

FIG. 7 shows the tensile test picture. Compared with 7a and 7b, it can be clearly seen that the state of the D-type curved surface sample before and after the failure, the fracture fracture is inclined, and the fracture position is up to 5.7mm. The maximum

load in the tensile elastic phase of the D-type sample is 82N, and the maximum fracture load is 75N, which is closely related to the special horizontal holes of D-type. Compared with FIG. 7c and FIG. 7d, the failure state of N-type samples is different from that of D-type samples, and the fracture fracture is horizontal. The result of this fracture mode is that the shape variable is large at the time of failure, but the maximum load in the elastic phase is only 11N at least, and the fracture load is only 10N. Although both type D and type N are brittle fractures, the horizontal pores of type D samples have less stress concentration and better overall tensile properties.

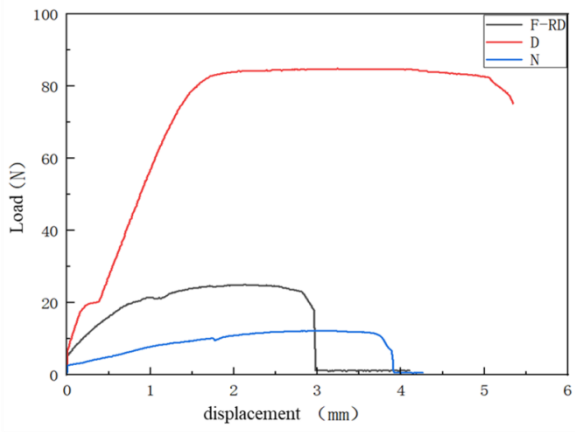

Figure.8. Experimental data of tensile model

As can be seen from Figure 8, we can observe that the stress-strain curve of the printed specimen mainly presents three obvious stages. The first is the elastic stage, in which the stress increases linearly as the strain increases. At this stage, the damage inside the specimen is less, and when unloaded, it will regain its shape without plastic deformation. The second is the yield stage, which is due to the flow of the slurry during the printing process resulting in the surface of the component and the fixture is not fully fitted, in a weak connection state, in this stage, the specimen will gradually fit the fixture with the increase of tensile stress, so there is a flat section. Finally, there is the fracture stage, in this stage, with the increase of strain, the stress no longer increases linearly, but suddenly decreases, resulting in a sudden fracture of the specimen. The fracture characteristics of the material show the characteristics of ductile fracture, which means that the material undergoes a certain degree of plastic deformation before the fracture occurs. Therefore, during the tensile process, the material exhibits a high tensile strength. By comparing the stress sizes of the three models under the same strain, we can obviously see that under the same strain, the stress required by D surface is the largest, indicating that D surface has the best tensile property.

3.3.2 Compression test results

Table 7 compressed sample model parameters

TMPS MODEL	SINGLE CELL SIZE /MM	POPULATION SIZE /MM	BULK VOLUME /MM3

D	2×2×2	115×25×2	3603
TMPS MODEL	Single cell size /mm	Population size /mm	Bulk volume /mm3
N	2×2×2	115×25×2	3603
F-RD	2×2×2	115×25×2	3603

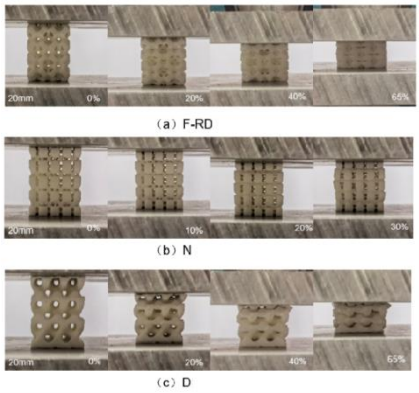

Figure.9. Compression test diagram (a. R-RD, b. N, & c. D)

Table 8 Compressed sample data table

TMPS Model	Elastic strain（%）	Elastic stress （MPa）	Compact strain （%）	Densification stress（MPa）	Maximum stress（MPa）
F-RD	7.2	4	55	8	13
D	12	6	55	8	13
N	4	2.5	15	5	13

It can be clearly seen from Figure 8 that the whole process of the three curved surface samples being compressed until they are destroyed. FIG. 9a shows the test compression process of FRD type samples. With large holes and small number of FRD surfaces, the compression strain can reach 7.2%, the elastic stress can reach 4Mpa, the dense strain can reach 55%, the dense stress can reach 8MPa, and the maximum bearing compressive stress is as high as 13MPa. Figure 9b shows the whole process of N-type sample compression to failure. N-type sample has small pores, large number of pores, and small communication channels between pores, which is easy to wrinkle. The compressive strain of N-type sample is only 4%, the elastic stress is only 2.5MPa, the dense strain is only 15%, and the dense stress is 5MPa. Figure 9c shows the whole process from compression to failure of Type D sample. Type D sample has the best compression performance, with the compressive strain reaching 12%, the elastic stress reaching 6Mpa, the dense strain reaching 55%, the dense stress reaching 8MPa, and the maximum bearing compressive stress reaching 13MPa. The holes of Type D sample are horizontal, the force is uniform, and the stress concentration area is small. Good overall compressive performance.

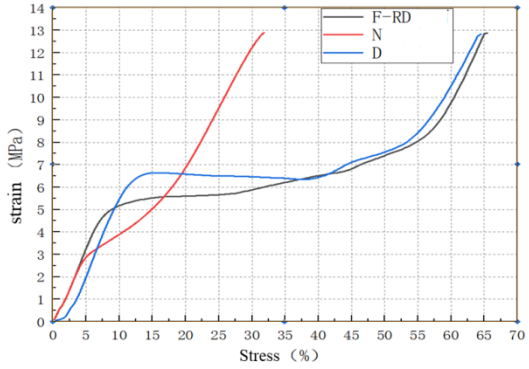

Figure.10. Compression model experimental data

The F-RD surface model and D-surface model made of PLA material can be divided into three stages, as shown in Figure 10, namely, the ascending stage, the gentle stage and the second ascending stage. However, the N-surface model only has two stages, namely, the ascending stage and the second ascending stage, and there is no gentle stage. In the first rise stage, all three models undergo elastic deformation, during which the model is subjected to a small load and bounces back to its original shape at the end of the load without permanent deformation. With the gradual increase of external load, the whole structure of the model does not change significantly, but a single cell begins to bend and deform. With the decrease of load, the displacement of TPMS structure increases gradually, which indicates that the TPMS structure has reached the maximum compressive strength. Even if the F-RD and D-type structures are destroyed, the cells can still provide a certain degree of compressive resistance. The degree of bending deformation increases when the cell is further damaged. In the compression area, instability occurs first, followed by the fracture of the fiber in the tension area, when the slip phenomenon occurs. The N-surface model does not appear at this stage because the cell is completely destroyed and does not provide a compressive effect. Subsequently, the load gradually increased due to the densification of PLA material. From this stress-strain curve, we can analyze that the compressive capacity of N surface is relatively poor, while the other two models have relatively good compressive capacity.

4. Conclusion

In this article, the mechanical properties of PLA materials with different TPMS structures were investigated through tensile and compression tests on TPMS structures, and the factors affecting the mechanical properties of printed specimens were analyzed. The main conclusions are as follows:

(1) The print specimen is divided into three stages in the whole tensile process, which are elastic stage, yield stage and fracture stage, and the failure form is brittle failure. Among them, the tensile properties of D structure are the best, while the tensile properties of F-RD structure and N structure are relatively poor.

(2) The printed specimen has two forms in the whole compression stage process,

F-RD structure and D structure have three stages, that is, the rising stage, the gentle stage, the second rising stage, and the N structure has only two stages, that is, the rising stage and the second rising stage. Among them, F-RD structure and D structure have relatively good compression performance, while N structure has poor compression performance. Through analysis, the failure mode of the 3D printed TPMS structure designed in this paper is the yield instability of the cell structure when it is subjected to out-of-plane compression load.

(3)The type D sample has horizontal pore type, the more uniform the stress is, and the lower the number of stress concentration sites in the same position interface, the better tensile and compressive properties. FRD sample has large pores, but the number is small, the force is more uniform, and the overall tensile and compressive properties are slightly lower than D sample. N-type samples have the largest number of pores, small pores and large distribution area. In the same section, there are many stress concentration locations, which seriously affect the tensile and compressive properties, so the N-type tensile and compressive properties are the worst.

The disadvantage of this paper is that there is no detailed comparison of a wide range of cavity TMPS models, and no comparison of mechanical properties of a single TMPS with different C values. The experiment provides some help for the study of TMPS.

Disclaimer (Artificial intelligence)

Option 1:

Author(s) hereby declare that NO generative AI technologies such as Large Language Models (ChatGPT, COPILOT, etc.) and text-to-image generators have been used during the writing or editing of this manuscript.

Option 2:

Author(s) hereby declare that generative AI technologies such as Large Language Models, etc. have been used during the writing or editing of manuscripts. This explanation will include the name, version, model, and source of the generative AI technology and as well as all input prompts provided to the generative AI technology

Details of the AI usage are given below:

1.
2.
3.

References

[1] Wu Haibo, WANG Xilun, FANG Yanxiong, et al. Development and Application of 3D printing catalytic materials [J]. Advances in Chemical Engineering, 2023, 42(08) : 3956-3964.

[2] Zhao Xiaojun. Application and clinical study of surgical guide made by

3D printing technology in immediate implantation [M].

[3] Wang Yang. Basic Research of hybrid additive manufacturing technology based on fused deposition molding 3D printing process [D], 2020.

[4] WASTI S,ADHIKARI S.Use of biomaterials for 3D printing by fused deposition modeling technique:a review[J].Front Chem,2020(8):315.

[5] BARDOT M,SCHULZ M D.Biodegradable poly(Lactic acid) nanocomposites for fused deposition modeling 3D printing[J].Nanomaterials(Basel),2020,10(12):2567.

[6] Hya B, Xza B, Gwa B, et al. Design optimization of a novel bio-inspired 3D porous structure for crashworthiness[J]. Composite Structures,2021, 255.

[7] A D L, A W L, A N D , et al. Optimal design and modeling of gyroid-based functionally graded cellular structures for additive manufacturing[J]. Computer-Aided Design,2018,104:87-9.

[8] Oraib K A ,Reza R ,N. A P , et al.On Mechanical Properties of Cellular Steel Solids With Shell-Like Periodic Architectures Fabricated by Selective Laser Sintering[J].Journal of Engineering Materials and Technology,2019,141(2).

[9] Maskery I ,Aremu A ,Parry L , et al.Corrigendum to “Effective design and simulation of surface-based lattice structures featuring volume fraction and cell type grading” [Mater. Des. 155 (2018) 220–232][J].Materials Design,2018,160106-107.

[10] Xue Yi-chi. Study on parametric design and mechanical properties of porous structures based on TPMS [D]. Huaqiao University,2022.

[11] Zhu Haolin, KANG Hanzi, ZHANG Haoyu, et al. Polylactic acid (POLylactic acid) plasticized by whole biofuranodiformate [J]. Engineering Plastics Applications, : 1-6.

[12] ORISEKEH D K, CORTI G, JAHAN M P. Enhancing thermo-mechanical properties of additively manufactured PLA using eggshell microparticle fillers [J]. Journal of

[13] Manufacturing Processes, 2025, 133: 782-797.

[14] Li Huaxiong, Wang Hui, Liu Xuan. Optimization of mechanical

properties of 3D printed PLA material by response surface method [J]. Plastic Science and Technology, 2024, 52(10) : 130-135. (in Chinese)

[15] Wu Haibo, WANG Xilun, FANG Yanxiong, et al. Development and Application of 3D printing catalytic materials [J]. Advances in Chemical Engineering, 2023, 42(08) : 3956-3964.

[16] WU S, YANG L, YAN C, et al. Fatigue properties of SiC graded ceramic lattice structures with a triply periodic minimal surface manufactured by laser powder bed fusion [J]. Journal of the European Ceramic Society, 2024, 44(15) : 116695

[17] HOMEM ALVES CéSAR RIBEIRO G, ROUZINEAU D, MEYER M, et al. Novel design approach based on triply periodic minimal surfaces (TPMS) for gas–liquid contactor packing [J]. Chemical Engineering Science, 2025, 304: 121062.

[18] LI K, ZUO C, LIAO R, et al. Optimizing mass transfer performance in triply periodic minimal surface porous scaffolds through isosurface offset [J]. Thin-Walled Structures, 2025, 208: 112800.

[19] Development status and trend of polymer materials for 3D bio-printing [J]. Advances in Materials in China,2018,37(12):949-969+993. (in Chinese)

[20] Li Xiao. Application of polylactic acid material in 3D printing technology [J]. Plastic Additives,2023,(04):70-73.

[21] LIU H, QIAN S, MEI D, et al. Numerical modeling of triply period minimal surface structures with catalyst coating for hydrogen production of methanol steam reforming [J]. International Journal of Hydrogen Energy, 2024, 69: 282-295.